Bulgarian Chemical Communications, Volume 44, Number 4 (pp. 356 – 363) 2012

Parametrization of impedance spectra of GC/H_2SO_4 electrode: trials and errors

V. Horvat-Radošević*, K. Magdić, K. Kvastek

Rudjer Bošković Institute, Bijenička c. 54, 10000 Zagreb, Croatia

Received February 20, 2012; accepted February 20, 2012

Impedance spectra of two differently prepared (polished and anodically oxidized) GC electrodes measured at +0.30 V *vs.* SCE in 0.5 mol dm^{-3} H_2SO_4 electrolyte have been analysed on the basis of presumed electrical equivalent circuit(s) and complex non-linear least square fitting procedure. Statistical analysis of model residuals and reliability of the estimated values of parameters were used as indicators for correct or incorrect modeling. In such a way, the polished GC electrode has been modeled using not-ideal capacitive element describing relatively flat surface, whereas anodically oxidized GC electrode has been modeled using not-ideal capacitive element loaded by transmision line element representing a porous surface structure.

Key words: GC electrodes, Electrochemical impedance spectroscopy, Electrical equivalent circuits, Parametrization

INTRODUCTION

It has already been shown that oxidized GC electrodes, like most of other carbon materials [1], exhibit high capacity values that become relevant even for advanced electrochemical double-layer capacitors [2, 3]. In that area, Electrochemical Impedance Spectroscopy, EIS, technique appears to be one of the principal methods for examining fundamental behaviour of electrode materials. This is primarily due to the possibility of EIS to estimate not only capacitance values, but also to follow charge transfer and transport related phenomena occurring at different time scales, what is essential for predictions of rate capabilities of capacitor devices [1, 4]. There are, however, only few studies available in the literature on the impedance analysis of GC electrodes. Although for a polarized carbon electrode, purely capacitive impedance response has generally been expected over broad potential region [1-4], more or less distributed capacitive response is found dominant for both: not activated and variously activated GC electrodes in different electrolyte solutions [2, 5-8]. Consequently, impedance models containing constant phase element(s), CPE, or transmission line, TL, have been discussed to account for roughness, including possible fractal geometry [5-8] or porosity of the GC surface [2].

The goal of the present paper was to find the optimum parameter set(s) of impedance spectra of not treated, *i.e. o*nly hand polished GC electrode, PGC, and anodically oxidized GC electrode, AGC, in H_2SO_4 electrolyte solution. Impedance analysis based on electrical equivalent circuits, EECs, involving lumped RC and/or distributed impedance elements [9] was applied and submitted to the statistical analysis of model residuals. The calculations were performed using the complex linear least square, CNLS, fitting procedure and modulus weighting mode [10, 11]. Improvements were made by replacement(s) and/or addition(s) of particular impedance(s) to the basic model and re-fitting this new model to the experimental data.

Criteria for finding the most reliable EEC were equal frequency distribution and small values of real and imaginary fitting residuals, Δ' and Δ'', defined as:

$$\Delta'_k = \frac{Z'_{k(\exp)} - Z'_{k(cal)}}{|Z_{k(\exp)}|} \qquad \Delta''_k = \frac{Z''_{k(\exp)} - Z''_{k(cal)}}{|Z_{k(\exp)}|} \quad (1)$$

In Eqn. (1), Z', Z'' and k are real and imaginary impedance and particular frequency of measurements, respectively. $|Z|$ is impedance magnitude, while by "*exp*" and "*cal*", experimentally measured and calculated quantities are denoted. A fit was considered good for fitting residuals, Δ' and Δ'', being below 0.01 and near equally distributed over the frequency region of impedance measurements.

EXPERIMENTAL IMPEDANCE SPECTRA

Bode plots (log of $|Z|$ and phase angle, φ *vs.* log ω, ($\omega = 2\pi f$) of PGC and AGC electrodes (0.028 cm^2

* To whom all correspondence should be sent:
E-mail: *vhorvat@irb.hr*

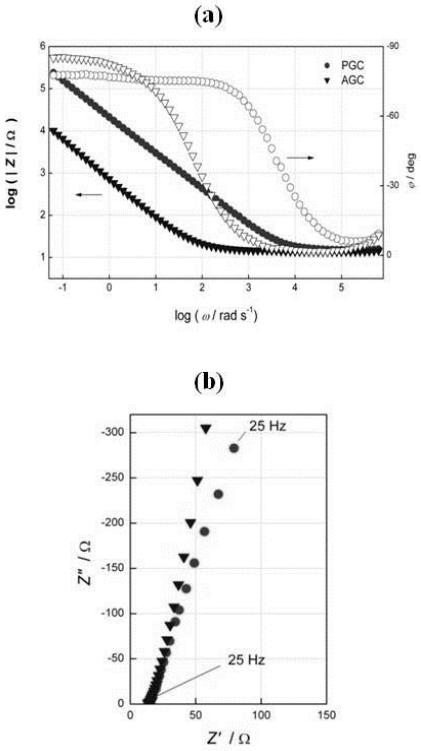

Fig. 1. Experimental IS of PGC and AGC electrodes in 0.5 mol dm^{-3} H_2SO_4 at +0.30 V *vs.* SCE: (a) Bode plots, (b) high to medium frequency parts of $Z^{''}$ *vs.* $Z^{'}$ plots

of apparent area) measured at +0.30 V *vs.* SCE using three-electrode cell filled with 0.5 mol dm^{-3} H_2SO_4 electrolyte solution are together with high frequency parts of $Z^{''}$ *vs.* $Z^{'}$ curves, presented in Fig. 1. Visual observation of experimental impedance spectra, IS, in Fig. 1a indicates two distinct domains, almost resistive response at higher and almost capacitive response at lower frequencies, respectively. Not prominent shifts of high frequency intercepts in Fig. 1b pointed to domination of the solution resistance, R_s = 13–15 Ω, over any contact and/or intrinsic resistance of GC electrodes. The values of $|Z|$ and degree of deviation from ideal capacitive response are higher for PGC than AGC electrode. The capacitance values, C_{IS}, calculated at f = 0.1 Hz using the relation $C_{IS} = -(\omega Z^{''})^{-1}$ are 5.15 × 10^{-5} F (1.8 mF cm^{-2}) for PGC and 1.90 × 10^{-3} F (68 mF cm^{-2}) for AGC electrode, respectively.

IMPEDANCE MODELING PROCEDURE

As is suggested by visual observation of IS in Fig. 1 and also by other authors [6-8], impedance response of GC electrodes can be associated with R_s and almost capacitive electrode impedance with frequency dispersed CPE having admittance, $Y_{CPE} = (Z_{CPE})^{-1}$, defined as:

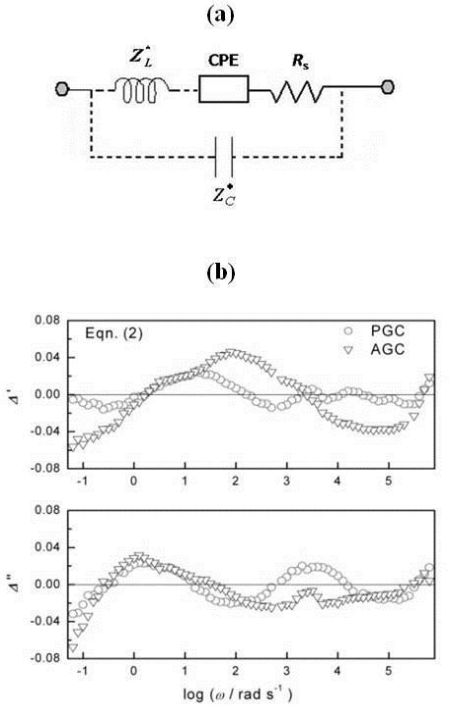

Fig. 2. (a) EEC with CPE defined by Eqn. (2) used for fittings to experimental IS of PGC and AGC electrodes in Fig. 1, (b) real and imaginary fitting residuals, $\Delta^{'}$ and $\Delta^{''}$, *vs.* log ω

$$Y_{CPE}(i\omega) = Q(i\omega)^n \qquad (2)$$

This model in the form of EEC is drawn in Figure 2a, together with, Z_L* and Z_C* involved for correction of experimental artefacts manifested at high frequencies [12, 13]. In all present experiments, L* = 4.1–6.0 × 10^{-6} H and C* = 4.2–5.7 × 10^{-8} F. EEC in Fig. 2a defines 3+2* model parameter-case (R_s, Q, n, L*, C*). The mean values of the extracted impedance parameters Q and n are together with their standard deviations, listed in Table 1.

Although for both electrodes, the results of fitting procedure of the EEC in Fig. 2a to IS in Fig. 1 yielded reasonable values for Q and n with low standard deviations, $\Delta^{'}$ and $\Delta^{''}$ were quite high and showed significant frequency dispersions (*cf.* Fig. 2b).

According to Figure 3, similar is obtained when CPE in Fig. 2a is replaced by the finite transmission line element, TL, with impedance defined as [9]:

$$Z_{TL}(i\omega) = \frac{R_0}{(i\omega\tau)^p}\coth(i\omega\tau)^p \qquad (3)$$

Generally, TL element with $Z_{TL}(i\omega)$ defined by Eqn. (3) can describe a situation within a porous

Table 1. The best fit main parameter values of the EEC in Fig. 2(a) with $Y_{CPE}(i\omega)$ defined by Eqn. (2).

	Parameter	PGC	AGC
3+2* parameter-case	104 × Q/Ω–1 sn	0.462 ± 0.001	17.42 ± 0.09
	n	0.856 ± 0.001	0.888 ± 0.002

Table 2. The best fit main parameter values of the EEC in Fig. 2(a) with CPE replaced by TL and $Z_{TL}(i\omega)$ defined by Eqn. (3).

	Parameter	PGC	AGC
4+2* parameter-case	R_0/Ω	3.8 ± 0.7	4.7 ± 0.4
	$10^3 \times \tau$/s	0.037 ± 0.009	4.6 ± 0.4
	p	0.4275 ± 0.0003	0.4464± 0.0007

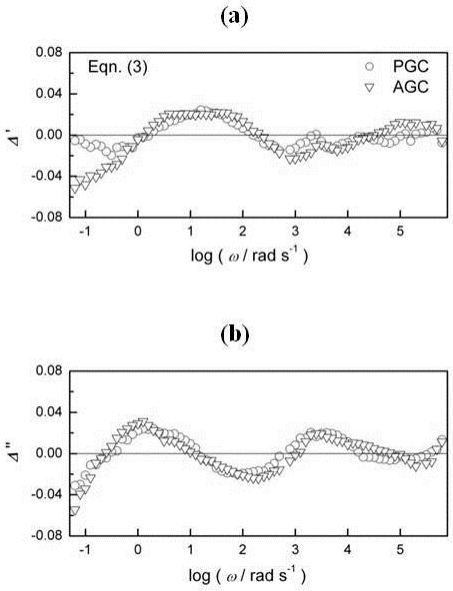

Fig. 3. Real and imaginary fitting residuals, Δ' and Δ'' obtained after fittings the EEC in Fig. 2(a) with CPE replaced by TL defined by Eqn. (3) to experimental IS of PGC and AGC electrodes in Fig. 1, *vs.* log ω.

electrode where the electrolyte resistance in pores is dependent not only on apparent conductivity of the electrolyte but also on a pore length [14]. This impedance/frequency function has already been applied in the impedance analysis of porous electrodes [14], including porous carbon [15] and anodically oxidized GC electrode [2]. In the ideal case of p = 0.5, impedance spectrum exhibits –45° inclined line at higher and –90° (capacitive) line at lower frequencies. Low frequency differential capacitance is defined here as $C_{LF} = \tau/R_0$, where τ is relaxation time, while R_0 represents resistance to ion transport.

By replacing CPE with TL having impedance defined by Eqn. (3), the model in Fig. 2a becomes 4+2* model parameter-case (R_s, R_0, τ, p, L*, C*). The mean values of the extracted parameters describing TL are, together with their standard deviations, listed in Table 2.

Although Eqn. (3) has already been proposed in impedance analysis of variously activated GC electrodes [2], use of TL instead of CPE in Fig. 2a did not improve results of fittings much. As is demonstrated in Fig. 3, fitting this model to the actual IS provided poor fits at large domain of measured frequencies. Therefore, for improving the results for GC electrodes, new impedance has to be added to the model. Generally, this can be done in two ways, what results with the well known problem of ambiguity in impedance data analysis [11, 16]. The first way is to add some new impedance that is capacitive at low frequency limit, in parallel connection to CPE (model P in Fig. 4a). The second is to add new impedance in a form of parallel *R*-CPE combination in series connection to CPE (model S in Fig. 4a).

For GC electrode, the P-type model has already been applied to account for some possible side reaction(s), including adsorption of electrolyte ions at the electrode surface [7,8]. On the other side, the S-type model is generally used to describe surface films with properties different than surrounding media (bulk electrode and electrolyte) [17]. For powdered carbon electrodes, the S-type model has also been proposed for accounting inhibition of charging/discharging of high carbon area surface caused by (bulk electrode/surface film or surface film/electrolyte) interfacial charge transfer [18, 19]. Somewhat modified S-type model, with two parallel CPEs, has already been proposed to account for different rates of charging/discharging at basal and edge planes of GC electroderespectively [5]. By replacing CPE with either P- or S-types of the models drawn in Fig. 4a, the EEC in

Fig. 2a becomes 6+2* model parameter-case (R_s, Q_1, n_1, R_1, Q_2, n_2, L*, C*). As is seen from decreased values of Δ' and Δ'' and their lower

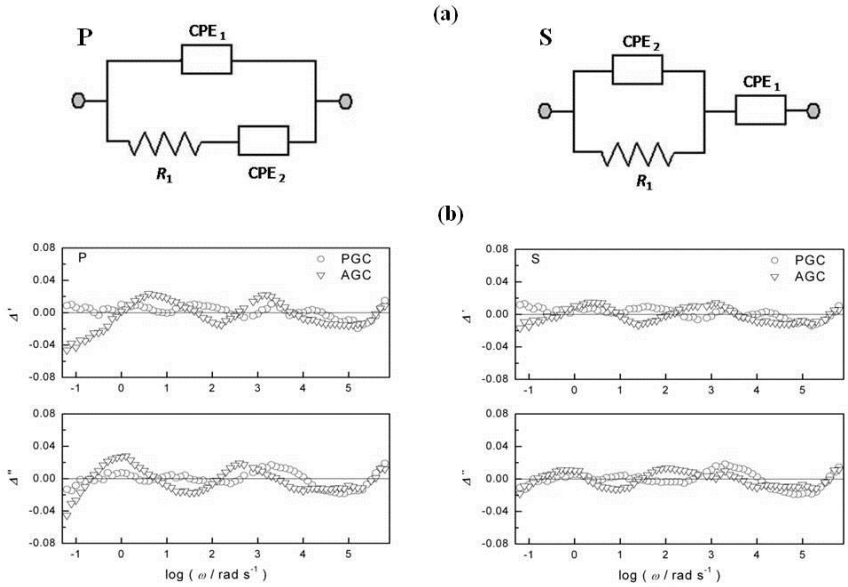

Fig. 4. (a) EECs used instead CPE in Fig. 2(a) for approximation of experimental IS of PGC and AGC electrodes in Fig. 1, (b) real and imaginary fitting residuals, Δ' and Δ'', *vs.* log ω

Table 3. The best fit main parameter values of the EEC in Fig. 2(a) with CPE replaced by the EECs in Fig. 4(a).

6+2* parameter-case	Parameter		PGC		AGC	
	P	S	P	S	P	S
$10^4 \times Q_1/\Omega^{-1}\,s^{n1}$	0.437 ± 0.003		0.474 ± 0.001		10.5 ± 0.5	
n_1	0.863 ± 0.001		0.869 ± 0.001		0.90 ± 0.06	
R_1/Ω	44152 ± 8274		373 ± 66		11 ± 9	
$10^4 \times Q_2/\Omega^{-1}\,s^{n2}$	0.0345 ± 0.003		4.9 ± 0.3		7 ± 5	
n_2	0.92 ± 0.03		0.82 ± 0.01		0.88 ± 0.08	
$10^4 \times Q_1/\Omega^{-1}\,s^{n1}$	0.437 ± 0.003		0.474 ± 0.001		10.5 ± 0.5	

frequency dispersions in Fig. 4b, these two models fit better to both experimentally measured IS in Fig. 1 when compared to the results obtained with previous models (*cf.* Figs. 2(b) and 3). Improvements of fits, however, are more pronounced after using the S-type model. The extracted main parameter values are together with their standard deviations summarized in Table 3. For either P- or S-type of the model, impedance of CPE_1 remained dominant impedance of each IS. For the PGC electrode, there are almost no differences between the values of parameters Q (n) in Table 1 and Q_1 (n_1) in Table 3, suggesting minor influence of additional impedance to the total electrode impedance. For the AGC electrode, however, additional impedance is found necessary for obtaining improvements in fitting results, suggesting thus more complex surface characteristics of this electrode. Although for the AGC electrode, the results using the S-type model yielded better fits with minor frequency dispersion (*cf.* Fig. 4b), unreasonable values for additional impedance were obtained (*cf.* Q_2 = 187 $\Omega^{-1}s^{n2}$ and n_2 = 0.59 in Table 3). This pointed to another type(s) of element(s) that should be used instead CPE_2 in the S-type of model. As has already been observed and discussed [1, 2], when carbon electrodes are polarized to high anodic potential, a porous surface with high content of oxygen containing species is formed. For that a reason, TL element, with impedance defined by Eqn. (4) and denoted here as TL_1, is included as additional element to either P or S-type of the model. These two new models that remain 6+2* model parameter-cases (R_s, Q_1, n_1, R_{01}, τ_1, p_1, L*, C*) are drawn in Fig. 5a and denoted as P-I and S-I.

Qualities of fittings are shown in Fig. 5b, whereas the main parameter values are, together

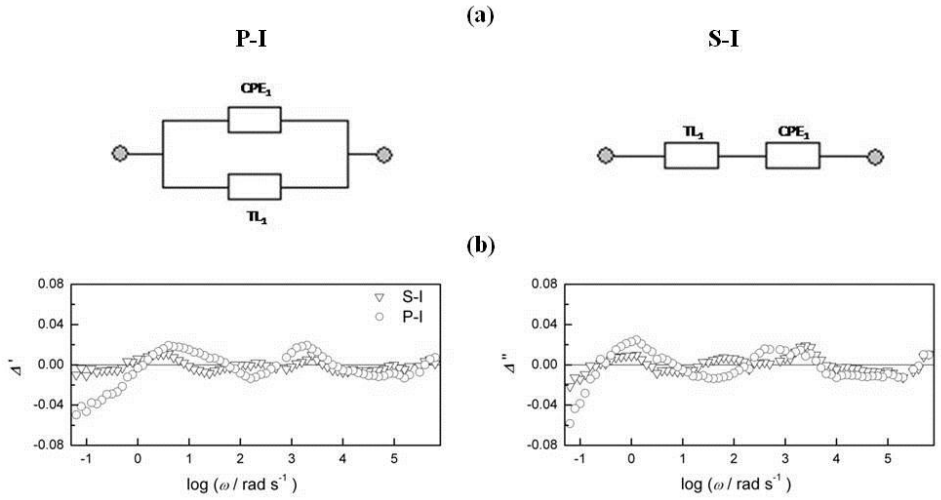

Fig. 5. (a) EECs used instead CPE in Fig. 2(a) for approximation of experimental IS of the AGC electrode in Fig. 1**,** (b) real and imaginary fitting residuals, Δ' and Δ'', *vs.* log ω.

Table 4. The best fit main parameter values of the EEC in Fig. 2(a) with CPE replaced by the EECs in Fig. 5(a)..

6+2*parameter- case	$10^4 \times Q_1/\Omega^{-1} s^{n1}$	n_1	R_{01}/Ω	τ_1 /s	p_1
P-I	8 ± 6	0.90 ± 0.09	20 ± 15	0.011 ± 0.004	0.44 ± 0.04
S-I	41 ± 5	0.68 ± 0.01	2.2 ± 0.2	0.006 ± 0.001	0.491 ± 0.006

with the corresponding standard deviations, listed in Table 4.

Again, high(er) quality of fitting for the S-I type model is observed in Fig. 5b. As a consequence of different ways of connection of two elements in P-I and S-I models respectively, contribution of CPE_1 to total electrode capacitance is higher for the P-I than for the S-I type of the model. This means that in the case of S-I type of the model, impedance due to CPE_1 becomes some sort of additional impedance to dominant impedance of TL_1.

High value of Q_1 and n_1 = 0.68 for the S-I type of the model in Table 4 suggests again that some element exhibiting "Warburg type" of frequency response (–45° sloped line) should be used as additional impedance to the dominant impedance of TL_1. It has already been shown [20] that deviations, frequently observed from medium to low frequencies after applying the Eqn. (3), can be corrected by adding a new TL element with impedance defined as [9]:

$$Z_{TL}(i\omega) = \frac{R_0}{(i\omega\tau)^p}\tanh(i\omega\tau)^p \qquad (4)$$

Series combination of Z_{TL} defined by Eqn. (4) and Z_{TL} defined by Eqn. (3) has already been applied in impedance analysis of thin conducting polymer films to account impedance of two mobile charge carriers [21-23]. Here, Z_{TL} defined by Eqn. (4) and denoted as TL_2 is added to Z_{TL} defined by Eqn. (3) and already denoted as TL_1, in both types of the model in Fig. 5a. For the P-I type of the model, however, over-parametrization becomes immediately evident by insensitivity of the calculation results on the impedance of CPE_1. Thus the P-I model becomes reduced to the series sum of two TL's (*cf.* Figure 6a), what is just the same situation obtained by substitution of CPE_1 with Z_{TL2} into S-I type of the model. By using the model in Fig. 6a instead CPE, the model in Fig. 2a becomes the 7+2* model parameter-case (R_s, R_{01}, τ_1, p_1, R_{02}, τ_2, p_2, L*, C*). Frequency dispersion of Δ' and Δ'' showing acceptable results of fittings are presented in Fig. 6c, while the values of extracted parameters are, together with their standard deviations, listed in the first raw of Table 5. The parameter values in Table 5 indicate that the total AGC electrode capacitance originates fully from TL_1. Due to relatively high τ_2, the contribution of the Warburg (–45° sloped line) part of TL_2 is prominent at mediate to low frequencies. What is observed not only here, but also elsewhere [22, 23], $\tau_1 \neq \tau_2$, what has not been predicted theoretically [21]. Interpretation, however, remains unclear, but full equivalence between impedance of the series sum of TL_1 and TL_2 and parallel sum of two TL_2 points toward possible interpretation in the terms of pores of unequal lengths [20]. Low τ_1 value makes TL_1 response almost capacitive, what could be a basis for decrease of the number of model parameters. In its reduced form, shown in Fig. 6b, the sum of TL_1 and TL_2 is reduced to the sum of

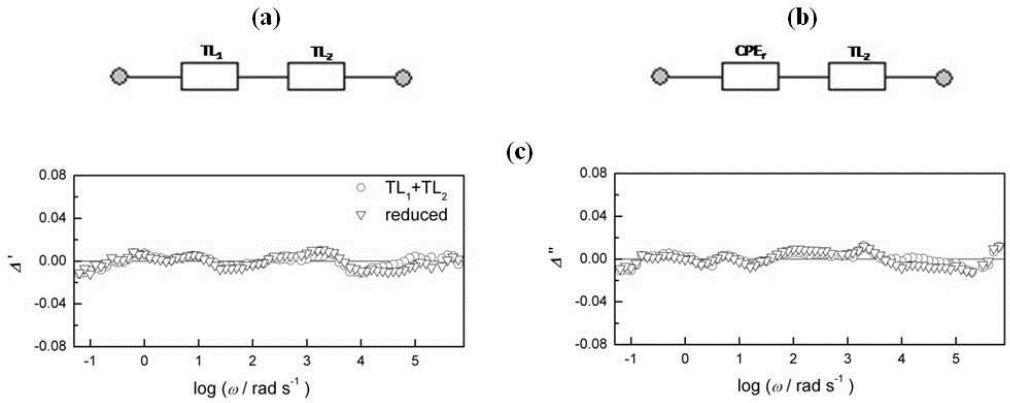

Fig. 6. (a-b) EECs used instead CPE in Fig. 2(a) for approximation of experimental IS of the AGC electrode in Fig. 1, (c) real and imaginary fitting residuals, Δ' and Δ'', *vs.* log ω.

Table 5. The best fit main parameter values of the EEC in Fig. 2(a) with CPE replaced by the EECs in Fig. 6a and b.

Parameters	R_{01}/Ω	$10^3 \times \tau_1$ /s	p_1	R_{02}/Ω	τ_2 /s	p_2
7+2* (Fig. 6a)	1.0 ± 0.1	1.0 ± 0.01	0.4594 ± 0.0005	22 ± 1	0.67 ± 0.05	0.50 ± 0.01
	--	$10^4 \times Q_r/\Omega^{-1}\,s^n$	n_r			
6+2* (Fig. 6b)	--	18.25 ± 0.02	0.921 ± 0.001	25 ± 1	0.75 ± 0.05	0.491 ± 0.008

CPE_r and TL_2. Now the model in Fig. 2a becomes reduced again to the 6+2* model parameter-case (R_s, C_r, n_r, R_{02}, τ_2, p_2, L*, C*). The results of fittings are also shown in Fig. 6c and the extracted parameter estimates are listed in Table 5. Very low residuals, randomly distributed over the range of measured frequencies and low standard deviation of each parameter value, point to the acceptable model used for fittings. This final model is checked through the potential dependence of measured IS of the AGC electrode, shown in Fig. 7 as the complex capacitance spectra, $Y'\omega^{-1}$ *vs.* $Y''\omega^{-1}$, that has already been found advantageous in visualization of not-ideal capacitive impedance responses of various origins [24].

Almost arc shaped curves in Fig. 7 exhibiting certain tails at lower frequencies, indicate a series connection of R_s and impedance of not ideal capacitive electrode. More or less prominent vertical lines observed at low frequencies for some potential values, indicate some additional and almost resistive contribution(s), probably due certain faradaic reaction(s) occurring at these potentials. The values of total electrode capacitances that can graphically be determined as the crossing points between the corresponding arcs and $Y''\omega^{-1}$ axis, show that the highest capacitance value is attained at +0.20 V, what is close to the redox potential of some oxygen containing, probably quinone-like surface groups, formed at carbon/H_2SO_4 (pH=0-3) electrodes [1,25]. Just the same is seen in Table 6, where the main parameter values estimates, including Q_1 (n_1) are listed. In such a way, the potential dependent contribution from the redox pseudocapacitance to the total electrode capacitance is approved. Changes of R_{02} and τ_2 values of TL_2 impedance in Table 6 show constant increase suggesting continuous change of the surface structure with increase of E. This, however, can have a detrimental effect when GC electrode is under conditions of continuous oxidation such as in capacitor devices.

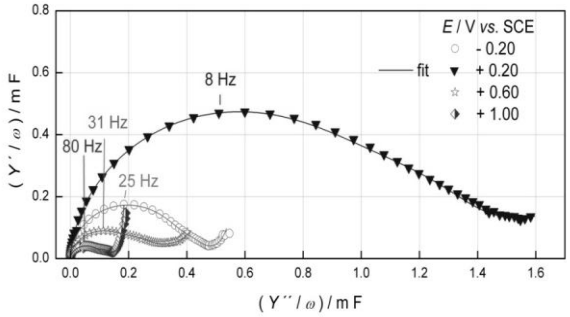

Fig. 7. Potential dependence of experimental complex capacitance spectra, $Y'\omega^{-1}$ *vs.* $Y''\omega^{-1}$, of the AGC electrode in 0.5 mol dm^{-3} H_2SO_4.

CONCLUSIONS

Experimental impedance spectra of polished, PGC and anodically oxidized, AGC, electrodes in H_2SO_4 electrolyte solution have been analysed using different EECs composed by gradual addition of different impedance elements. Statistical analysis of model residuals and

Table 6. The best fit main parameter values of the EEC in Fig. 2(a) with CPE replaced by the EEC in Fig. 6(b) to experimental IS of AGC electrode measured at various potentials

E/V *vs.* SCE	$10^4 \times Q_1/\Omega^{-1} s^n$	n_1	R_{02}/Ω	τ_2 /s	p_2
–0.20	4.76 ± 0.01	0.958 ± 0.001	14 ± 5	0.4 ± 0.3	0.39 ± 0.02
+0.20	13.99 ± 0.03	0.952 ± 0.001	25 ± 1	0.46 ± 0.04	0.431 ± 0.006
+0.60	3.322 ± 0.005	0.922 ± 0.001	23 ± 1	0.077 ± 0.007	0.450 ± 0.007
+1.00	1.55 ± 0.03	0.939 ± 0.001	49 ± 2	0.068 ± 0.004	0.492 ± 0.006

reliability of parameter estimates have been used as indicators for correct/incorrect modelling.

It has been shown that PGC electrode can be analysed as the 3+2* model parameter-case (not ideal capacitive element in series with electrolyte resistance), describing relatively flat electrode surface of PGC with some degree of roughness or fractal-scaled imperfections.

AGC electrode showed more complex behaviour and impedance analysis was based on more comprehensive model. While there was not a fundamental reason that one EEC is more significant than the other, several different types of EECs were applied and all were reduced to the 6+2* model parameter-case (not ideal capacitive element loaded by an impedance of distributive type). This model suggests a porous surface structure of AGC made by anodic oxidation and formation of high quantity of oxygen containing surface groups.

Acknowledgements. *Financial support from Ministry of Science, Education and Sports of the Republic of Croatia (Project 098-0982904-2905) is acknowledged.*

REFERENCES

1. B. E. Conway, Electrochemical Supercapacitors, Scientific, Fundamentals and Technological Applications, Kluwer Academic/Plenum Publ. New York (1999).
2. M. G. Sullivan, R. Kötz, O. Haas, J. *Electrochem. Soc.* **147** , 308, (2000).
3. Y. Wen, G. Cao, Y. Yang, *J. Power Sources* **148,** 121, (2005).
4. R. Kötz, M. Carlen, *Electrochim. Acta* **45,** 2483, (2000).
5. P. Heiduschka, A. Munz, W. Göpel, *Electrochim. Acta* **39,** 2207, (1994).
6. C.-H. Kim, S.-I. Pyun, J.-H. Kim, *Electrochim. Acta* **48,** 3455, (2003).
7. S. S. Moganty, R. E. Baltus, D. Roy, *Chem. Phys. Letters* **483,** 90, (2009).
8. J. P. Zheng, P. C. Goonetilleke, C. M. Pettit, D. Roy, *Talanta* **81,** 1045, (2010).
9. R. R. Macdonald (Ed.), Impedance Spectroscopy, Wiley, New York, 1987.
10. B. A. Boukamp, *Solid State Ionic*s **169,** 169, (2004).
11. P. Zoltowski, *Solid State Ionics* **176,** 1979, (2005).
12. S. Fletcher, *Electrochem. Commun*. **3,** 71, (2001).
13. V. Horvat-Radošević, K. Kvastek, *J. Electroanal. Chem.* **631,** 10, (2009).
14. R. De Levie, Adv. Electrochem. Electrochem. Eng., Vol. 6. Interscience, New York, 1967.
15. J. H. Jang, S. M. Oh, *J. Electrochem. Soc*. **151,** A751, (2004).
16. V. Freger, S. Bason, J. Membrane Sci. **302,** 1, (2007).
17. M. D. Levi, D. Aurbach, *J. Phys. Chem. B* **101**, 4630, (1997).
18. K. Sawai, T. Ohzuku, *J. Electrochem. Soc*. **144,** 988, (1997).
19. M. Toupin, D. Bélanger, I. Hill, D. Quinn, *J. Power Sources* **140,** 203, (2005).
20. M. D. Levi, C. Wang, D. Aurbach, *J. Electroanal. Chem.* **561,** 1, (2004).
21. M. A. Vorotyntsev, L. I. Daikhin, M. D. Levi, *J. Electroanal. Chem*. **364,** 37, (1994).
22. G. Láng, M. Ujvári, G. Inzelt, *J. Electroanal. Chem*. **572,** 283, (2004).
23. V. Horvat-Radošević, K. Kvastek, M. Kraljić-Roković, *Electrochim. Acta* **51,** 3417, (2006).
24. T. Pajkossy, D. M. Kolb, *Electrochim. Acta* **53,** 7403, (2008).
25. H. Andreas, B. E. Conway, *Electrochim. Acta* **51,** 6510, (2006).

ОПРЕДЕЛЯНЕ ПАРАМЕТРИТЕ НА ИМПЕДАНСНИТЕ СПЕКТРИ НА GC/H_2SO_4 ЕЛЕКТРОД: ПРОБИ И ГРЕШКИ

В. Хорват - Радошевич, К. Магдич, К. Квастек

Институт Руджер Бошкович, Биженичка 54, 10000 Загреб, Хърватска

Постъпила на 20 февруари, 2012 г.; приета на 20 февруари, 2012г.

(Резюме)

Импедансните спектри на два подготвени по различен начин (полиран и анодно оксидиран) стъкловъглеродни електрода, измерени при +0.30 V спрямо SCE в електролит от 0.5 mol dm^{-3} H_2SO_4 са анализирани въз основа на предполагаеми електрически еквивалентни схеми и комплексна процедура на нелинейно напасване по метода на най-малките квадрати. Като индикатори за правилното моделиране е използван статистически анализ на остатъците в модела и анализ на надеждността на оценените стойности на параметрите. По такъв начин, полираният стъкловъглероден електрод е моделиран чрез неидеален капацитивен елемент, описващ сравнително гладка повърхност, докато анодно оксидираният стъкловъглероден електрод е моделиран чрез неидеален капацитивен елемент, свързан с елемент на дълга линия, представящ пориста структура на повърхността.